Patch-scale representation of vegetation within hydraulic models

Timothy I. Marjoribanks,[1,2]* Richard J. Hardy,[2] Stuart N. Lane[3] and Matthew J. Tancock[4]
[1] School of Civil and Building Engineering, Loughborough University, Loughborough, UK
[2] Department of Geography, Durham University, Durham, UK
[3] Institute of Earth Surface Dynamics, Faculté des géosciences et de l'environnement, Université de Lausanne, Lausanne, Switzerland
[4] JBA Consulting, Skipton, UK

*Correspondence to: Timothy I. Marjoribanks, School of Civil and Building Engineering, Loughborough University, Loughborough, LE11 3TU UK.
E-mail: t.i.marjoribanks@lboro.ac.uk

Earth Surface Processes and Landforms

ABSTRACT: Submerged aquatic vegetation affects flow, sediment and ecological processes within rivers. Quantifying these effects is key to effective river management. Despite a wealth of research into vegetated flows, the detailed flow characteristics around real plants in natural channels are still poorly understood. Here we present a new methodology for representing vegetation patches within computational fluid dynamics (CFD) models of vegetated channels. Vegetation is represented using a Mass Flux Scaling Algorithm (MFSA) and drag term within the Reynolds-averaged Navier–Stokes Equations, which account for the mass and momentum effects of the vegetation, respectively. The model is applied using three different grid resolutions (0.2, 0.1 and 0.05 m) using time-averaged solution methods and compared to field data. The results show that the model reproduces the complex spatial flow heterogeneity within the channel and that increasing the resolution leads to enhanced model accuracy. Future applications of the model to the prediction of channel roughness, sedimentation and key eco-hydraulic variables are presented, likely to be valuable for informing effective river management. © 2016 The Authors. Earth Surface Processes and Landforms published by John Wiley & Sons Ltd.

KEYWORDS: vegetated channels; eco-hydraulics; computational fluid dynamics; drag

Introduction

Submerged aquatic vegetation is abundant in many lowland river systems and exerts a strong influence on the functioning of the fluvial system. Vegetation, through the additional flow resistance it generates, influences water depth, mean flow velocities (Jarvela, 2002; Green, 2005a; Nepf *et al.*, 2007) and turbulence (Okamoto and Nezu, 2009; Nikora, 2010), which subsequently affects sediment dynamics (Dawson, 1981; Sand-Jensen *et al.*, 1989; López and García, 1998), water quality (Kadlec and Knight, 1996; Ghisalberti and Nepf, 2006) and habitat diversity (Westlake, 1975; Liu *et al.*, 2008). Consequently, research has investigated the effects of vegetation on flow, but predominantly focussing on: single plants (e.g. Siniscalchi and Nikora, 2013; Albayrak *et al.*, 2014); idealized patches and canopies (e.g. Ghisalberti and Nepf, 2002; Okamoto and Nezu, 2009; Marjoribanks *et al.*, 2014b; Meire *et al.*, 2014); or the modification of roughness parameters at the larger scale (e.g. Kouwen and Unny, 1973; Green, 2005b; Shucksmith *et al.*, 2011).

Flow data around real vegetation patches in natural channels are relatively scarce (Naden *et al.*, 2006). Field studies have measured vegetation and flow at the patch-scale but these have focussed primarily on velocity profiles around and above single patches (Naden *et al.*, 2006; Sukhodolov and Sukhodolova, 2010) or descriptive analysis of the spatial patterns of flow structure (Cotton *et al.*, 2006). However, flow adjustment around vegetation patches controls the magnitude of form drag exerted on the flow. This in turn determines the flow resistance as well as the extent of wake regions that introduce process heterogeneity, promote sedimentation and provide habitat for terrestrial and aquatic wildlife (López and García, 1998; Kemp *et al.*, 2000; Liu and Shen, 2008). Thus the physical processes driving flow–vegetation interactions at the patch-scale need to be fully understood to explain how vegetation affects both spatial and temporal flow dynamics and hence river morphodynamics, eco-hydraulics and stream biogeochemistry.

Current models for predicting the effect of vegetation on flow in natural channels focus predominantly on the effects of vegetative resistance on reach-scale hydraulic parameters such as mean bulk velocity and flow depth. The models are often dependent upon physically-based empirical relationships using roughness parameters (e.g. Ferguson, 2007) and do not provide information on the spatial patterns of flow structure (Green, 2005b; Baptist *et al.*, 2007; Folkard, 2011; Marjoribanks *et al.*, 2014a). Verschoren *et al.* (2016) highlight the potential for modelling spatial flow patterns around vegetation patches, though their model still relies upon roughness parameters and

uses a simplified flow model. Computational Fluid Dynamics (CFD) has the potential to provide additional insight into flow-vegetation interactions within natural channels where intensive flow measurement can be problematic but this requires improved models of the interactions between vegetation and river flow (Marjoribanks *et al.*, 2014a).

The aim of this paper is to develop and to apply a new methodology for representing vegetation patches within a low-resolution CFD methodology that enables the prediction of the effect of vegetation on spatial flow patterns. Such information is crucial in assessing the impact of vegetation on hydraulics, sediment transport and stream ecosystems and permits holistic river management. We suggest herein that a predictive model should not be dependent on empirical calibration, but instead rely upon a physical process representation of flow–vegetation interaction. The specific objectives of this paper are: (1) to develop a physically-based vegetation model within a CFD framework; (2) to assess the predictive capability of the model and the impact of spatial resolution on flow prediction as compared with field data; (3) to apply the model alongside a bare channel case in order to examine the impact of vegetation on flow and to extract key hydraulic, geomorphological and ecological variables.

Field Methodology

Field site

In order to obtain the necessary boundary conditions and validation data, field data were collected from the River Browney in Durham, northern England. The reach was chosen due to its relatively simple cross-section and planform shape and the abundance of submerged vegetation. The river reach flows through agricultural land with a stream gradient of ~0.0035. This reach of the river had a predominantly gravel bed (D_{50} = 0.036 m, D_{84} = 0.0783), with a significant amount of coarse boulder material. The vegetation was dominated by *Ranunculus penicillatus* with one additional reed patch (*Phragmites* spp.) and riparian vegetation along both banks. At the time of survey, the riparian vegetation was predominantly overhanging from the bank and therefore not considered. However, it did inhibit surveying of the river edge in parts. The average flow depth was approximately 0.2 m.

Data collection

In order to produce a digital elevation model (DEM) as a boundary condition for the CFD simulation, topographic data were collected using a Total Station electronic distance meter (EDM). Measurements were taken at a series of cross-sections approximately 0.2 m apart in the downstream direction, with a similar separation between points in the cross-stream direction. The resulting DEM had a point density of between 20 and 50 points per square metre throughout the channel. Based upon previous work, this has been shown to obtain a good representation of gravel bed rivers with less than 15% loss of information (Lane *et al.*, 1994). The DEM (Figure 1) shows a relatively even bed with a slight pool at the end of the domain.

Vegetation positions were geo-located by mapping the outline shape of each patch using the Total Station EDM. These outlines were converted into polygon vegetation maps and then mapped onto a raster for insertion into the numerical model. In addition, the mean submergence depth of each patch was recorded, with the caveat that this will be spatially and temporally variable for each patch.
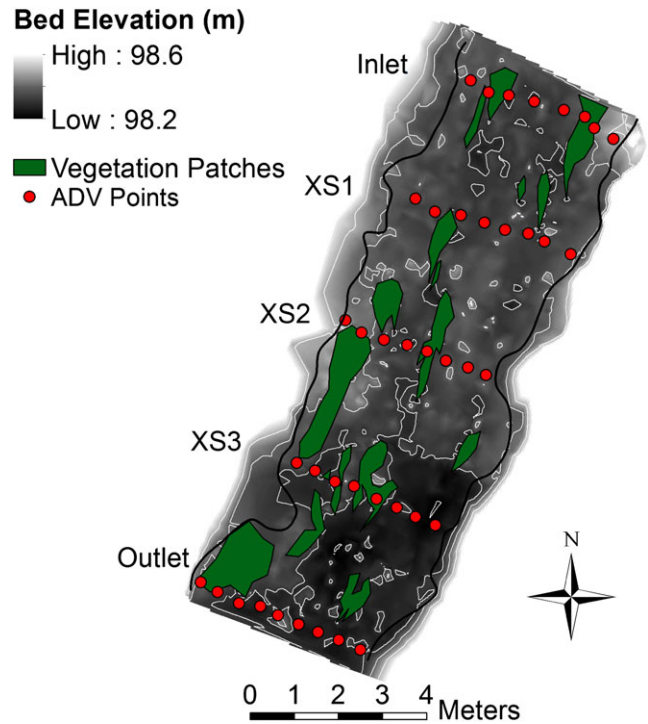

Figure 1. Field setup. Green patches represent vegetation, red circles show acoustic Doppler velocimeter (ADV) points and the contour map shows the topography. [Colour figure can be viewed at wileyonlinelibrary.com]

Flow measurements were taken using a Sontek acoustic Doppler velocimeter (ADV) at five cross-sections including the inlet and outlet of the domain, during steady discharge, to provide both boundary conditions and validation data (Figure 1). Each time series was collected for one minute, at 10 Hz resolution, to provide a stationary time series (Buffin-Bélanger and Roy, 2005). Velocity measurements were taken at 0.4 of the depth, in order to obtain a depth-averaged velocity estimate at each location.

Numerical Methodology

Flow modelling

Flow was modelled by solving the three-dimensional Navier–Stokes equations using a finite-volume approach. Here we use the Reynolds-averaged (RANS) form of the mass and momentum equations (Equations (1) and (2)) obtained by splitting the flow variables into time-averaged ($\overline{u}$) and fluctuating (u') components such that $u = \overline{u} + u'$. In Equations (1) and (2), p is the pressure, u is the three-dimensional velocity vector ($u = [u_x\ u_y\ u_z]$), x is the corresponding Cartesian co-ordinate vector ($x = [x\ y\ z]$), ρ is the fluid density and μ is the dynamic viscosity.

$$\frac{\partial \overline{u_i}}{\partial x_i} = 0 \qquad (1)$$

$$\frac{\partial \overline{u_i}}{\partial t} + \overline{u_j}\frac{\partial \overline{u_i}}{\partial x_j} = \frac{1}{\rho}\frac{\partial p}{\partial x_i} + \frac{1}{\rho}\frac{\partial}{\partial x_i}\left(\mu \frac{\partial \overline{u_i}}{\partial x_i} - \rho \overline{u_i' u_j'}\right) \qquad (2)$$

All of the terms in Equation (2) are expressed as time-averaged quantities with the exception of the final terms, the Reynolds stresses, which originate from the product of the fluctuating velocity components. There is no direct way of calculating these terms and solving the RANS equations requires use of

© 2016 The Authors. *Earth Surface Processes and Landforms* published by John Wiley & Sons Ltd.

Earth Surf. Process. Landforms, Vol. **42**, 699–710 (2017)

a turbulence closure scheme to model the effects of turbulent Reynolds stresses (Lane, 1998). Using the Boussinesq approximation (Boussinesq, 1877) the Reynolds stresses can be related to time-averaged velocity gradients and an eddy viscosity term (v_t) (Keylock *et al.*, 2005; Sotiropoulos, 2005) (Equation (3)).

$$- \overline{u_i' u_j'} = v_t \left(\frac{\partial \overline{u_i}}{\partial x_j} + \frac{\partial \overline{u_j}}{\partial x_i} \right) \tag{3}$$

There are many approaches to calculating the eddy viscosity (see Sotiropoulos, 2005). The most common is the two-equation $k - \varepsilon$ model that relates the eddy viscosity to the ratio of turbulent kinetic energy (k) and dissipation (ε), both of which must be solved using additional transport equations. Here we use the $k - \varepsilon$ Re-Normalization Group (RNG) turbulence closure model (Yakhot and Orszag, 1986), which has been adopted in geomorphological applications due to its improved performance in regions of high strain and flow separation compared to the standard $k - \varepsilon$ model (Lien and Leschziner, 1994; Hodskinson and Ferguson, 1998; Bradbrook *et al.*, 2000; Ferguson *et al.*, 2003).

The RANS equations are solved using the SIMPLEST algorithm (Spalding, 1980) whereby the velocity field is solved using the momentum equation (Equation (2)) and then a pressure correction is applied to solve the mass equation (Equation (1)) ensuring a divergence-free velocity field. This process of solving for momentum and then correcting for continuity is repeated iteratively until a converged solution is obtained. The convergence criterion was set such that the residuals of mass and momentum flux were reduced to 0.1% of the inlet flux.

Discretization and boundary conditions

The domain was 13 m long (l), 7 m wide (w) and 0.4 m high (h). In order to evaluate the effect of discretization on the performance of the vegetation models, each model was applied with three different spatial resolutions (Δx): 0.05 m ($nx = 260$, $ny = 130$, $nz = 8$); 0.1 m ($nx = 130$, $ny = 70$, $nz = 4$); and 0.2 m ($nx = 65$, $ny = 35$, $nz = 2$) where nx, ny and nz are the number of grid cells in the x, y and z directions, respectively. These three resolutions are referred to as 'high', 'medium' and 'low' resolutions. This enabled investigation of the effect of spatial resolution on process representation and therefore resolution requirements for accurate simulation of the reach. For each simulation, a regular Cartesian grid was used and the bed topography was interpolated onto a raster and represented using a mass flux scaling algorithm (MFSA) approach. The MFSA allows the inclusion of complex mass blockages within a regular Cartesian grid through the alteration of cell porosities. This approach was first proposed by Olsen and Stokseth (1995) and was developed further by Lane *et al.* (2002, 2004). The advantage of this approach is that it allows inclusion of complex boundaries without the need for grid distortion that can lead to increased artificial diffusion and numerical instability (Hardy *et al.*, 2005).

The sub-grid grain-scale drag acting at the bed was represented using a combined MFSA and drag force method as outlined by Carney *et al.* (2006) using $D_{84} = 0.0783$ m as the representative grain size. The free surface was represented using a rigid-lid approximation based on the average water surface measured along the reach.

The inlet data were linearly interpolated from the time-averaged ADV readings, and all three time-averaged velocity components, as well as the kinetic energy, were specified at the inlet. The time and space averaged inlet velocity and kinetic energy were used throughout the domain to initialize the simulation and aid convergence.

Vegetation model

The vegetation was represented using both an MFSA to account for the mass blockage of the vegetation and a drag force term that was implemented as a momentum sink term in the Navier–Stokes equations (e.g. Wilson and Shaw, 1977; Fischer-Antze *et al.*, 2001; López and García, 2001). The finite volume continuity equation has the form:

$$f_c = \frac{\sum_k a_k f_k}{a_c + S} \tag{4}$$

where f is the variable of interest (u_i) the index c represents the value at the cell centre, the index k represents the values at neighbouring cell centres and the previous time-step and S is the linear source coefficient. The neighbour links (a_k) have the form

$$a_k = A_k \phi \rho u + D + T \tag{5}$$

where A_k is the cell-face area, ϕ is the cell-face porosity, ρ is the fluid density, u is the local velocity perpendicular to the face and D and T are diffusion and transient terms, respectively. Thus, in order to introduce the MFSA, the value of ϕ is altered at each face according to the presence of vegetation and was calculated as the solid volume fraction, assuming an equal distribution of vegetation mass:

$$\phi = M \pi r_p^2 \tag{6}$$

Here, M is the stem density (per square metre of the bed) and r_p is the stem radius (in metres). The average stem density was estimated as 10 000 stems m^{-2} and the stem radius was estimated as 0.0015 m based on field observations. This represents a solid volume fraction of ~0.07, which is in agreement with observed values for aquatic vegetation canopies (Nepf *et al.*, 2013). To introduce the momentum sink term, the drag force per unit mass was calculated using Equation (7) (Nepf, 1999) and the linearized source term, ($S = F_D / f_c$) was therefore calculated using Equation (8).

$$F_D(f_c) = 0.5 C_D M 2 r_p f_c^2 \tag{7}$$

$$S = C_D M r_p \left| f_c^* \right| \tag{8}$$

In these equations, C_D is the dimensionless drag coefficient, and $\left| f_c^* \right|$ is the magnitude of the currently stored value of the variable of interest (u_i). In the converged solution, $f_c^* = f_c$ and therefore the correct source term is calculated. The drag coefficient was taken as one, in line with previous studies (Kim and Stoesser, 2011).

Vegetation locations were geo-located within the domain using the patch location and submergence depth. It was assumed that each patch of vegetation filled the height of the domain up to its measured canopy top height. In the upper most vegetated cell, where the vegetation did not occupy the entire cell, the drag force and MFSA values were scaled linearly accordingly to the percentage of the cell that was considered vegetated. Cells above the canopy top were treated as free from vegetation.

Previous studies have sought to model the additional sub-grid turbulent kinetic energy production due to vegetation (e.g. López and García, 2001). However, this requires calibration for different flow situations. It has also been shown that in natural channel flows, the sink terms dominate the turbulent diffusive terms (Fischer-Antze *et al.*, 2001; Stoesser *et al.*, 2003). Therefore, the turbulence effects of vegetation were not included within the Navier–Stokes equations.

Methodological Approach to Comparison of Field and Model Data

In order to compare the modelled data and the field data, we apply both a reach-scale and a single point hydraulic comparison. At the reach-scale, we compare the Manning's *n* roughness values, which directly correspond to the water surface slope.

Using Equation (9) the water surface slope (S_0) is extracted (Nicholas, 2001) from the model data and used to calculate the Manning's *n* roughness value using Equation (10).

$$S_0 = \frac{1}{\rho g} \frac{dp}{dx} \tag{9}$$

$$n = \frac{R^{\frac{2}{3}}}{U} S_0^{\frac{1}{2}} \tag{10}$$

Here the hydraulic radius ($R = A/P$) is estimated based on the domain average, calculated using the numerical model cross-sections to obtain the cross-sectional area (A) and wetter perimeter (P). The mean downstream velocity (U) is averaged over the wetted domain. For the field data, the bed topography and depth measurements at the ADV locations are used to calculate the water surface slope and the mean velocities are averaged over the ADV locations.

In order to compare single point velocities between the field and numerical data, three-component velocities are sampled from the model across three cross-sections (Figure 1), excluding the inlet and outlet. To get an idea of the spatial performance of the model, we analyse the cross-stream variation in downstream and cross-stream velocity predictions from the models. This has the benefit that it is able to identify the ability of the model to reproduce the overall flow structure rather than simply replicate individual point values. The velocity data at each (x, y) location across the model domain are averaged over all the fluid cells in the vertical (z) direction to obtain a depth-averaged velocity across the whole domain. Depth-averaged, downstream velocity is used as the primary variable for analysis as this is the most useful indicator for conveyance. However, cross-stream velocities are also presented.

Performance of the models is quantified using mean absolute error (MAE) values between the modelled and observed velocities at the ADV measurement locations. MAE was chosen as this metric provides a representative error estimate that is less skewed by the presence of a few very large error values that may not relate to model prediction error. Within highly heterogeneous flows such as those with sharp flow gradients associated with vegetation shear layers, geolocation errors within the ADV data can cause high apparent errors in velocity. To account for this, we compare the ADV data not just to the single corresponding point measurement within the numerical simulation, but to modelled values over a small spatial window around the exact measurement location (0–0.4 m) along the cross-section, and analyse how the minimum MAE varies with window size (δ). We anticipate two effects of this analysis. Firstly, errors in geolocation will lead to a sharp decrease in minimum
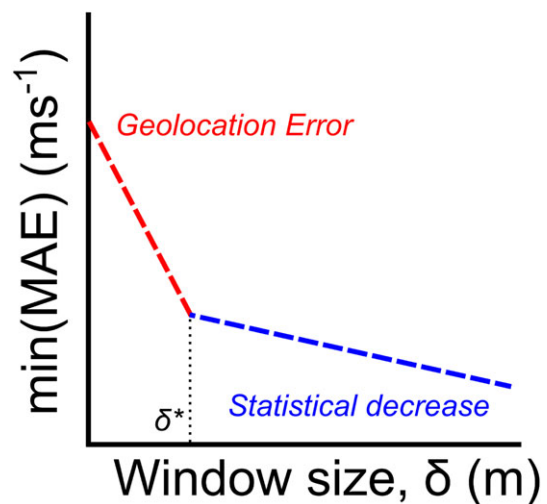

Figure 2. Schematic diagram of expected variation in minimum mean absolute error (MAE) with window size (δ). The red dashed line indicates the decrease in error due to geolocation error while the blue dashed line indicates the more gradual decrease in error due to statistical effects. The black dotted line illustrates the theoretical threshold value (δ^*) between these two regimes. [Colour figure can be viewed at wileyonlinelibrary.com]

MAE (Figure 2) over a window size that is representative of the likely error magnitude in geolocation of measurements and flow features within the simulation [e.g. global positioning system (GPS) errors]. Secondly, minimum MAE will statistically decrease with increasing window size, due to the increase in data points providing a larger random distribution of values against which to compare the data. This will produce a more gradual decrease (Figure 2). Therefore, the window size is selected based upon visual examination of the results to identify a threshold value (δ^*) that captures the majority of geolocation errors while minimizing the impact of the statistical effect.

While we anticipate that this will diminish the impact of geolocation error, a conservative choice of spatial window may not account for large geolocation errors. Therefore, having applied a spatial window we visually characterize remaining errors into three categories (Figure 3). Firstly, remaining errors due to geolocation are likely to be characterized by consistent lateral shifts in both downstream and cross-stream velocities at a single velocity measurement location. Secondly, errors due to model performance, including the effects of parameterization and the limitations of the model itself are likely to be represented by consistent deviation from the field data across multiple locations. Thirdly, errors in field data collection due to performance of the measurement equipment are likely to involve single locations where the model deviates from the field data, in contrast to neighbouring points. These three categories provide qualitative categorization of the errors. However, we note that it is not possible to verify these assumptions and it is likely that errors may cumulate across all three categories.

We use both the reach-scale and point-scale comparisons to assess the impact of grid resolution ($\Delta x = \Delta y = \Delta z$) on predicted flow velocity, by comparing predictions of the vegetation model across three grid resolutions to the ADV data collected in the field. The objective here is not to perform a grid independence study for model verification (Hardy *et al.*, 2003) as at such low resolution we do not expect the solution to be grid-independent, if it is possible to talk about grid independence when applying CFD to a continuously-varying but measurement-sampled surface: as a grid is refined, it is likely to resolve flow around the topographically sampled surface and not the real surface. Instead, the goal is to assess the impact of grid resolution (and by extension topographic
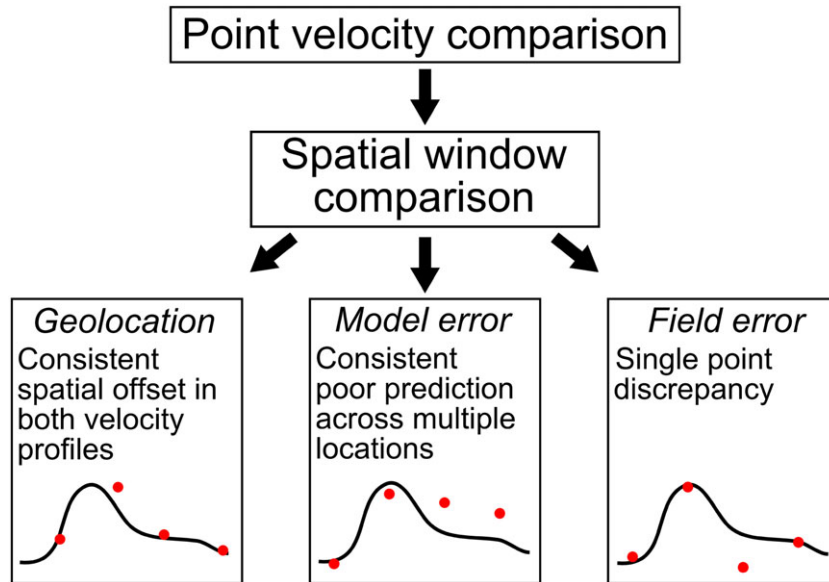
Figure 3. Error mitigation and classification process. Small geolocation errors are mitigated through use of a spatial window comparison. Remaining errors are then classified into three types (geolocation, model error and field error) based upon visual comparison of the flow profiles. The three schematic diagrams show hypothetical modelled (black lines) and measured (red circles) velocities. [Colour figure can be viewed at wileyonlinelibrary.com]

and vegetation patch resolution) on the solution and to evaluate the degree to which the representation of key features such as wakes and recirculation regions is sensitive to grid resolution.

Model Assessment

First we consider the reach-scale predictive capability of the model across the three resolutions. The measured Manning's n value for the reach is $n = 0.075$. Comparing the results of the three different resolution models (Table I) shows that the high resolution model performs best with less than 5% error, and that the error value increases with grid size. The medium resolution model gives an error of 6.7% while the low resolution model produces an error of 16.3%. These results demonstrate a significant increase in reach-scale predictive capability with resolution, particularly between the low and medium resolution cases. However, the trend is not straightforward. For the medium and low resolution cases, the model over-predicts the Manning's n value whereas the high resolution model under-predicts the roughness.

Comparing the single point velocity measurements, the plot of MAE against window size for the downstream velocity (Figure 4) shows that by simply considering the single data points, errors range between 0.06 and 0.11 m s^{-1}. The data point at ~1 m in XS2 was excluded from the error analysis as it was identified to be an erroneous field measurement based upon the magnitude of the mean and fluctuating velocity signal in comparison to similar points. There appears to be a decreasing impact of window size on MAE with initial sharp drop-off and then a more gradual decrease in error that is consistent

with the pattern predicted in Figure 2. It is not possible to define an exact threshold value δ^* between these two regimes. However, based upon visual inspection of Figures 4 and 5 we suggest that a spatial error window of 0.1 m (~0.5–2Δx, ~0.014w) captures the majority of geolocation errors whilst minimizing the impact of the statistical decrease with window size (i.e. $\delta < \delta^*$). Assuming a maximum spatial error of 0.1 m, the errors are between 0.04 and 0.09 m s^{-1}. There is a clear improvement in prediction with increasing grid resolution with over 50% reduction in error between the low and high resolution models. This pattern is consistent across all window sizes.

For the cross-stream velocities, the errors at the ADV points at different resolutions are more similar with values between 0.040 and 0.045 m s^{-1} (Figure 5). Similar to the downstream velocities, there is an initial sharp drop-off in error with window size and within a 0.1 m spatial window, the velocity errors fall to 0.025–0.035 m s^{-1}. There is evidence of increased predictive capacity with grid resolution and this is most marked between the low and medium resolution models. Applying the spatial error window of 0.1 m there is little difference in error

Table I. Comparison of Manning's n values calculated in the field with those obtained from the three different resolution numerical models

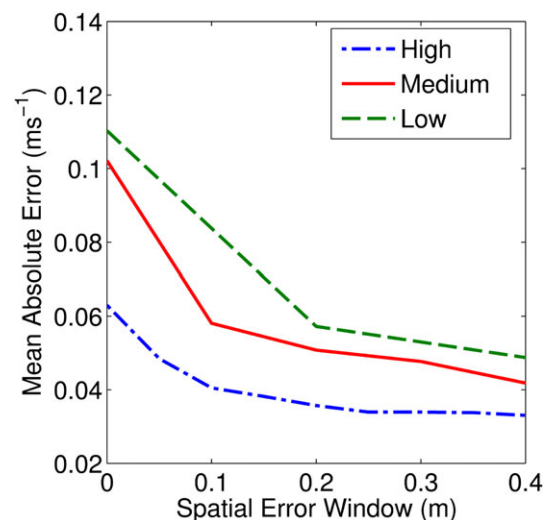| Case	Manning's n	Error
Field measurement	0.0748	—
Low (0.20 m)	0.0870	16.3%
Medium (0.10 m)	0.0798	6.7%
High (0.05 m)	0.0712	4.8%

Figure 4. Variation in mean absolute error in downstream velocity with spatial error window. [Colour figure can be viewed at wileyonlinelibrary.com]
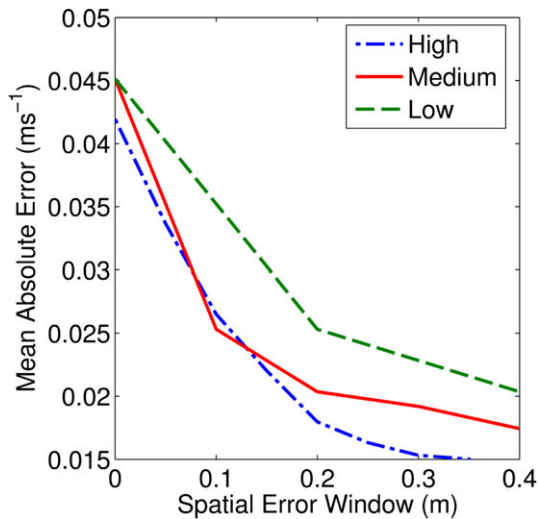
Figure 5. Variation in mean absolute error in cross-stream velocity with spatial error window. [Colour figure can be viewed at wileyonlinelibrary.com]

($\sim$0.001 m s^{-1}) between the medium and high-resolution models.

The point value comparisons by cross-section (Figure 6) show that the model is able to reproduce the key visual features of cross-stream variation in depth-averaged downstream velocity at all three cross-sections. It is encouraging that even at cross-section 3 (XS3), the farthest downstream from the inlet, complex flow patterns are still being reproduced within the model, suggesting that the model performance reflects accurate process representation and not simply propagation of the measured inlet boundary conditions.

Within the cross-section profile data (Figure 6) we identify three broad patterns of interest. First, there are regions where model performance is enhanced gradually with increased resolution. This is in agreement with the results in Figure 4 and is particularly evident between 1 and 3 m in XS1. This pattern suggests that model errors (Figure 3) are causing systematic errors at lower resolution. Second, there are regions where an increase in resolution leads to a sudden dramatic improvement in predictive capability. This can be seen at 1 m and 4 m in XS1. In both cases, with an increase from medium to high resolution, there is a decrease in error of $>$0.1 m s^{-1}. Similarly, we characterize these as model errors that most likely relate to the inadequate representation below certain resolutions of flow processes
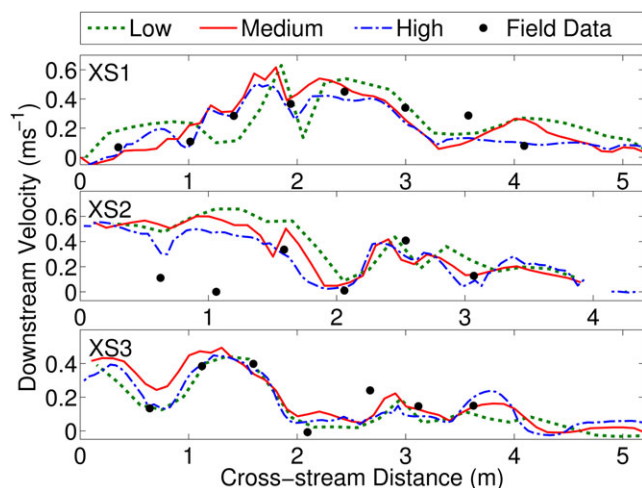
related to topographic or vegetative forcing. Third, there are regions where all models perform equally well, but there is large discrepancy between the observed and predicted data. This can most clearly be seen at $\sim$3.6 m in XS1, between 0 and 1 m and at $\sim$2.6 m in XS2, and at $\sim$2.7 m in XS3. In XS1, using the high resolution model data we characterize this error as field measurement error due to the lower error at both neighbouring points. For 0 to 1 m in XS2, given the large error ($>$ 0.2 m s^{-1}) across neighbouring measurement points, we also characterize this error as model error. Given the consistency of error between resolutions and the location of the ADV points in shallow, unvegetated free-stream flow (see Figure 1), we suggest this error may be due to specification of the boundary conditions (e.g. bed surface and free surface). However, we do note the decrease in error at $\sim$0.6 m at the highest resolution which suggests it is possible that there is also a discretization effect.

At both $\sim$2.6 m in XS2 and $\sim$2.7 m in XS3, there appears to be a lateral shift in the downstream velocity peak and therefore it is possible that these errors are due to geolocation. The cross-stream velocity profile for XS2 (Figure 7) shows a similar spatial offset at $\sim$2.6 m to that observed for the downstream velocity and therefore the error is most likely to be due to geolocation. For XS3, there is no similar evidence of an offset in the cross-stream velocity profile. Instead, the corresponding point shows an isolated large error in cross-stream velocity across all resolutions ($>$ 0.05 m s^{-1}) and therefore we suggest that this is most likely due to field measurement error.

Similar to Figure 6, the cross-stream velocity profiles (Figure 7) highlight distinct areas of the flow where prediction is visually good, such as 3 to 4 m in XS1 (Figure 7) with errors $<$0.01 m s^{-1} for the high resolution model. Here, the improvement between the low and medium resolution models is clear. Similar improvement is also seen across XS2. Conversely, there are sections in XS3 where the low-resolution model appears to perform best (0–1 m, 3–4 m). There is no evidence of systematic under- or over-prediction of velocity magnitudes by the model, as the models appear to over-predict at XS2 and under-predict velocity magnitude at XS1.

These results demonstrate that in spite of errors the vegetation model is capable of predicting the complex flow profiles within the channel. Even at the coarsest resolution the model is able to reproduce large wake structures. However, there are also clear thresholds in grid resolution and process representation. Increasing the grid resolution enables improved accuracy in predicting velocity patterns and magnitudes, reducing downstream velocity errors by approximately 33% between resolutions.
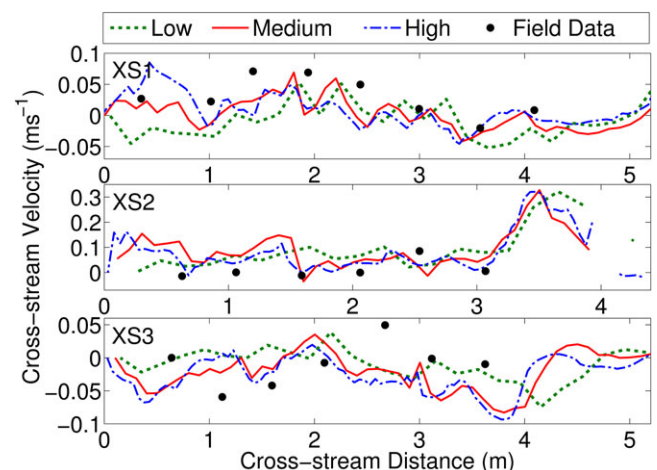

Figure 6. Downstream velocity profiles at cross-sections 1, 2 and 3 (XS1, XS2 and XS3) for low, medium and high resolution. [Colour figure can be viewed at wileyonlinelibrary.com]

Figure 7. Cross-stream velocity profiles at cross-sections 1, 2 and 3 (XS1, XS2 and XS3) for low, medium and high resolution. [Colour figure can be viewed at wileyonlinelibrary.com]

Application of the Model to Understanding Reach-scale Processes

Having assessed the performance of the model across a range of grid resolutions, we now use the high resolution model results to discuss the impact of vegetation on channel processes, as compared to an unvegetated, bare channel. In particular, we consider the impact of vegetation on (i) flow hydraulics; (ii) sediment deposition and morphodynamic evolution; and (iii) habitat and ecology (eco-hydraulics).

Flow hydraulics

The depth-averaged velocity plots for the unvegetated and vegetated channel cases (Figures 8 and 9) show that the presence of vegetation within the channel increases small-scale variability but dampens the impact of large regions of flow recirculation. In the unvegetated case, the main channel is predominantly homogeneous except for a number of very narrow (width < 0.2 m) topographically-induced wake structures. In contrast, in the vegetated case, there is increased spatial variation in downstream velocity, with the formation of much wider wake regions (width > 0.4 m) behind individual vegetation patches. The maximum and minimum velocities across the domain do not change as these are reached away from the locations of vegetation patches. However, the distribution of downstream velocities across the domain for the vegetated case (Figure 10a) shows a significantly different distribution (Kolmogorov–Smirnov test, $D^* = 0.1762$, $p < 0.05$) with much higher occurrence of velocities substantially above and below the mean velocity compared with the unvegetated case. This demonstrates the effect of vegetation patches (seen in Figure 8) in creating subchannels and high velocity threads (as identified by Gurnell *et al.*, 2006) within the main channel. The result is a bimodal distribution of velocities (Figure 10a) where the domain-averaged velocity ($U \approx 0.2$ m s^{-1}) fails to describe either of the two dominant flow regimes: wake flow and high velocity threads.

For the depth-averaged cross-stream velocities (Figure 9) there is also a clear visual impact of the vegetation, introducing
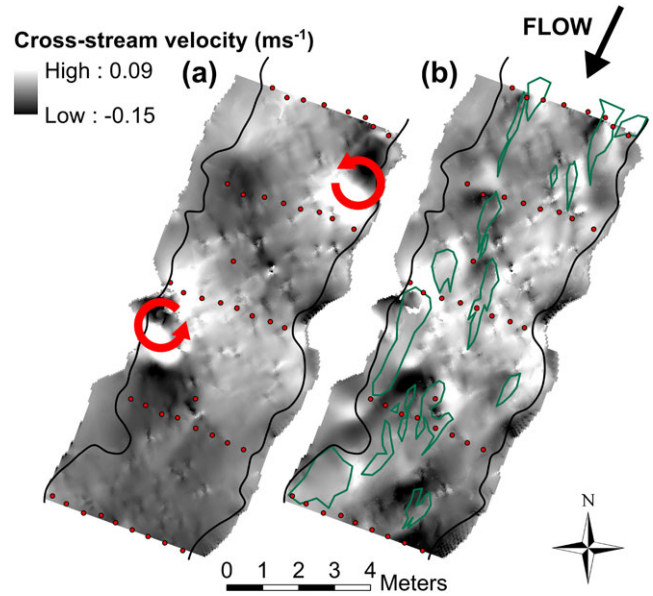

Figure 9. Depth-averaged cross-stream velocity predictions for the (a) unvegetated and (b) vegetated channel. Vegetation patches shown in green. Flow recirculation regions shown in red. [Colour figure can be viewed at wileyonlinelibrary.com]

more variability in cross-stream velocities within the channel. The distribution of cross-stream velocities is visually more similar between the vegetated and the unvegetated channels than for the downstream velocities (Figure 10b), but there is still a significant difference between the distributions (Kolmogorov–Smirnov test, $D^* = 0.1474$, $p < 0.05$).

Figure 9a highlights the presence of large-scale domain-induced recirculation regions, for example just downstream of the inlet on the true left of the channel, which appear stronger in the unvegetated channel and introduce large cross-stream velocities. Therefore, although the vegetation introduces smaller-scale patch velocity variations, it also decreases the effect of larger-scale channel-induced secondary circulation. In addition, the vegetated domain exhibits sharp spatial downstream velocity gradients (Figure 8) with many lateral canopy shear layers evident across the domain that will create shear layer turbulent structures and contribute significantly to the turbulent kinetic energy budget.

It is non-trivial to generalize the observed vegetation wake structures due to their complex shape in comparison to those used to investigate vegetation wake flows in the flume environment (e.g. Chen *et al.*, 2012; Meire *et al.*, 2014). However, it is clear from Figure 8 that there is not a simple relationship between patch width or length and wake length with a wide range of patterns evident. For example, there are similar sized patches that exhibit noticeably different strength wakes (patches labelled in Figure 8). This is due to the impact of neighbouring patches as well as orientation, bed topography and complexity of patch shape, which will all confound the underlying relations found in idealized conditions.

At the reach-scale, the model provides insight into the effect of vegetation on channel roughness. In order to highlight the impact of the model on predicting vegetative roughness, we extract the prediction of n_4, the component of the roughness relating directly to vegetation (Cowan, 1956), by subtracting the roughness of the unvegetated channel case. This assumes that the two primary sources of roughness in the channel are the bed friction and vegetation and that the vegetative roughness is additive (Cowan, 1956; Green, 2005a). This approach produces an estimate of $n_4 = 0.0225$. Given the qualitative nature of many estimates of vegetative roughness in the literature and the variation in measured roughness even within same
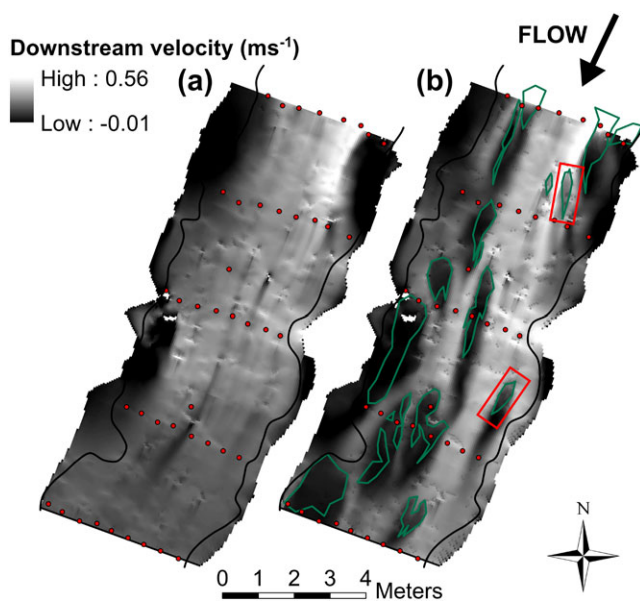

Figure 8. Depth-averaged downstream velocity predictions for the (a) unvegetated and (b) vegetated channel. Vegetation patches shown in green with two similar patches shown in red boxes. [Colour figure can be viewed at wileyonlinelibrary.com]
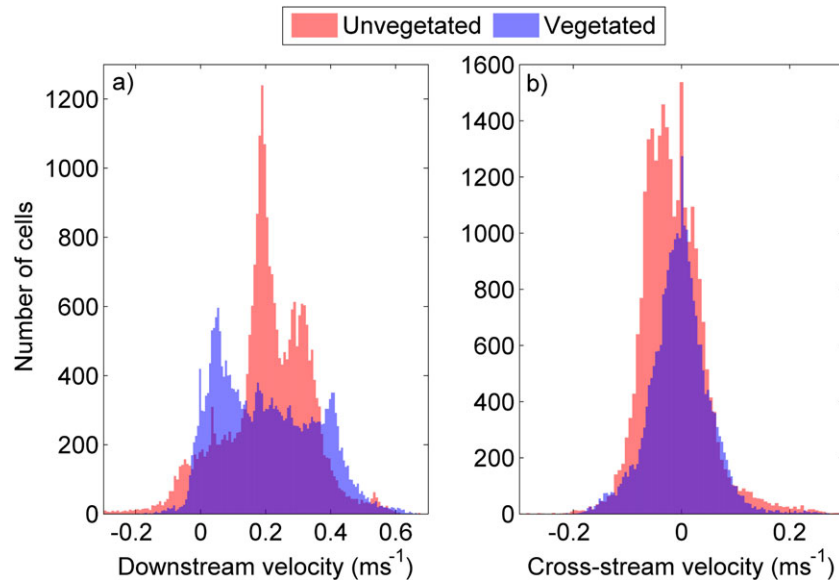
Figure 10. Distribution of depth-averaged velocities across the domain for the unvegetated (red) and vegetated (blue) cases. [Colour figure can be viewed at wileyonlinelibrary.com]

vegetation species across different sites (O'Hare *et al.*, 2010), it is difficult to validate this value directly. However, the value lies within the 'medium' vegetated case according to Chow (1959). We suggest these results highlight the model's ability to predict with accuracy the effect of vegetation on channel hydraulics. In particular, the data requirements for model prediction do not greatly exceed those of the existing models that exhibit similar or greater errors (e.g. Fisher, 1992; Green, 2006).

Sediment deposition and morphodynamic evolution

Using the spatial velocity data from the model it is possible to infer patch-induced fine sediment deposition patterns (de Lima *et al.*, 2015). In this approach, sedimentation regions are identified using a critical threshold velocity, below which sediment deposition may occur. This velocity threshold will vary depending on grain size and represents a simplified approach to sediment transport. Applying the threshold velocity of de Lima *et al.* (2015) ($u_c = 0.0475 \, \mathrm{m \, s^{-1}}$) and thereby assuming similar grain sizes to those used by Chen *et al.* (2012) (~0.012 mm), a sedimentation map is created (Figure 11). Although in this case the map refers to an arbitrary grain size, the results demonstrate the key impacts of vegetation on inferred sedimentation patterns. The presence of vegetation increases the percentage of the domain exhibiting sedimentation from 13% to 18% due to the presence of sedimentation regions both in, and behind vegetation patches.

These regions of fine sediment and organic matter accumulation may provide favourable conditions for vegetation growth and therefore may determine vegetation configuration and landscape evolution (Gurnell *et al.*, 2005; Meire *et al.*, 2014). Furthermore, the presence of vegetation removes some predicted sedimentation zones due to the effect of vegetation patches deflecting flow towards the banks. This can be clearly seen near the inlet at both edges of the channel. This highlights some potential for vegetation to increase bank erosion (Gurnell *et al.*, 2006).

Habitat and ecology

Spatially distributed velocity data are a key component in predicting availability and suitability of habitat. Typically, the
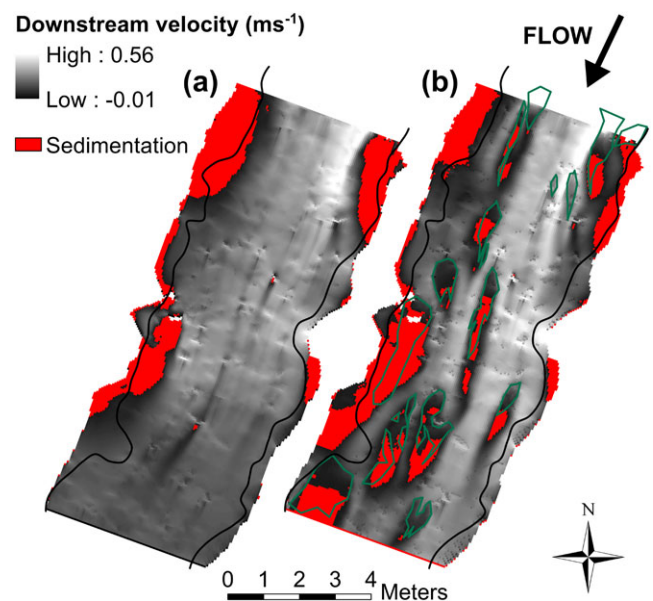

Figure 11. Inferred deposition patterns for the (a) unvegetated and (b) vegetated channels using the approach of de Lima *et al.* (2015). Areas of deposition are shown in red. Vegetation patches shown in green. [Colour figure can be viewed at wileyonlinelibrary.com]

criteria applied to generate a habitat suitability index (HSI), from which the weighted usable area (WUA) can be calculated are the flow velocity, depth and channel properties (Bovee, 1978; Leclerc, 2005). This approach assumes that the distribution of biota is controlled by the hydraulic conditions within the water column (Gore and Hamilton, 1996). The presence of vegetation within the channel has been shown here to introduce heterogeneity within the channel that alters the distribution of downstream velocities (Figure 10), which will in turn impact significantly on the WUA calculation.

In addition, the spatial flow data permit calculation of key eco-hydraulic metrics that have been proposed for quantifying stream habitat, including kinetic energy gradient (KEG) and vorticity (Crowder and Diplas, 2000, 2006). KEG reflects the rate at which the drag force acting on a fish will change between two locations and identifies ideal feeding locations where fish rest in relatively slow regions adjacent to faster flow that transports food (Kozarek *et al.*, 2010). Similarly, vorticity highlights

regions of high velocity gradient and has been shown to increase dissolved oxygen levels within the flow (Cokgor and Kucukali, 2004). The comparison of KEG (Figure 12) between the unvegetated and vegetated channels demonstrates the impact of vegetation patches in increasing energy gradients, and thus increasing the availability of ideal hydraulic conditions for fish. Hydraulic preferences will vary with species and age, but applying the ideal habitat condition of Crowder and Diplas (2006) for brook trout (4 < KEG <14), the vegetated channel shows a 69% increase in optimal feeding conditions.

Similarly, the vorticity plots (Figure 13) show the impact of flow around individual vegetation patches in creating regions of high positive and negative vorticity. The mean absolute vorticity magnitude for the vegetated channel (0.42) is almost double that of the unvegetated channel (0.23), again demonstrating the increased flow complexity due to the presence of vegetation, which may enhance fish habitat within the channel.

Discussion

The results demonstrate that the vegetation model developed here is able to reproduce both the spatial patterns and magnitudes of the velocity profiles, even reproducing complex wake structures and high velocity threads (Gurnell *et al.*, 2006). There is a clear improvement in predictive capacity with spatial complexity (grid resolution) although the degree of improvement is spatially dependent and less pronounced between the high and medium resolution cases. The key finding of this work is the ability of the model to produce spatially distributed hydraulic data, which provides a means for assessing the impact of vegetation on channel processes. Application of the model has highlighted the impact of vegetation patches on velocity distributions and flow structure, inferred erosion and deposition processes and eco-hydraulic metrics. Such spatial information is not available from existing methods that account for vegetation through a reach-averaged vegetative roughness term or rely on simplified flow models.

While the model shows good agreement with field data for many of the ADV locations, there are a number of locations where prediction appears poorer. As discussed, these may relate to either error in geolocation, field measurement or model
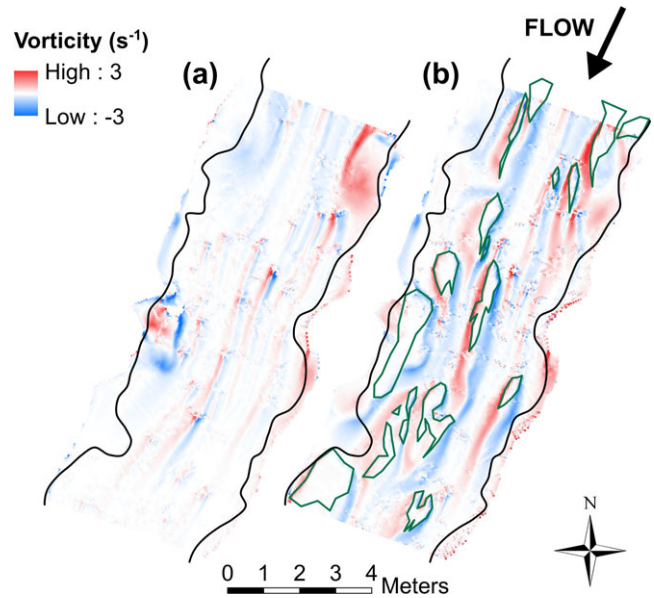

Figure 13. Vorticity plots for the (a) unvegetated and (b) vegetated channels. Vegetation patches shown in green. [Colour figure can be viewed at wileyonlinelibrary.com]

discretization and parameterization. Geolocation errors in the field data collection methodology may have affected the vegetation position mapping, DEM creation and location of validation velocity data. The EDM relies upon the measuring pole being vertical, and even variations in angle from the vertical by as little as 2° can introduce horizontal positional errors of 0.06 m. This is particularly significant in heterogeneous flows such as vegetated channels where steep velocity gradients occur across the vegetated boundaries and associated wakes (Sand-Jensen, 1998; Wilson *et al.*, 2005). This error was mitigated in part by the use of the error window in calculating the MAE.

Field measurement errors include errors in the ADV measurement due to the reflection from vegetation and bed elements within the measurement volume as well as unrepresentative velocity measurements. For example, the low grid resolution and consequent large grid cell volume (1.3×10^{-4} to 8.0×10^{-3} m^3) of the models is problematic when comparing field data obtained over a much smaller sampling volume (2.5×10^{-7} m^3). Here, due to the order of magnitude difference in sampling volume, point data obtained in the field may not be representative of the mean flow over the surrounding region. Furthermore, velocity data were collected at 0.4 of the depth, which was between 0.04 and 0.12 m from the bed. At distances so close to the bed it is likely that individual large grain-induced flow structures may have affected velocity values ($D_{84} = 0.0783$ m).

Finally, with respect to model parameterization, the vegetation model is dependent on patch characteristics such as submergence depth, solid volume fraction (a function of stem density and diameter) and drag coefficient. Submergence depth and stem diameter were measured manually within the field and are thus subject to measurement error and were also assumed constant across patches. Currently, there is a lack of available data on plant characteristics such as plant geometry and solid volume fraction (Green, 2005b) and there is a need to collect such information across a range of common macrophytes to enable continued development of CFD models such as the one introduced here. In particular, the drag coefficient is known to be inaccurate, and increasing model accuracy and transferability between field sites through a more effective estimation of drag coefficients within such complex environments is a key avenue for future research (Fischer-Antze *et al.*, 2001; Kim and Stoesser, 2011). However, in this specific case
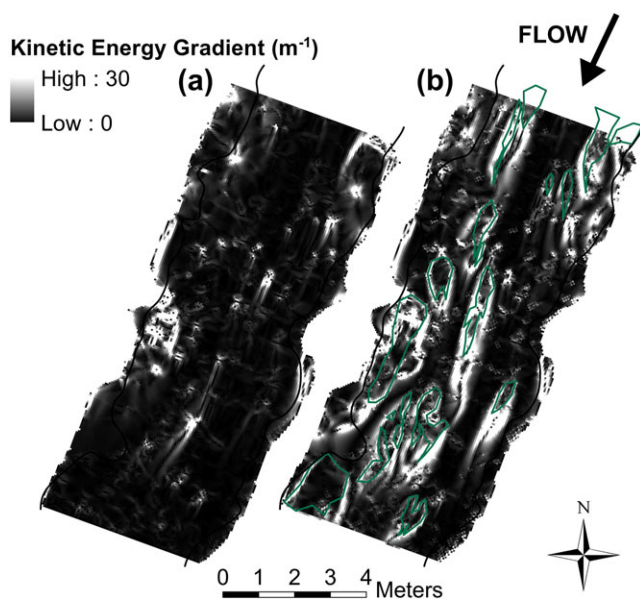

Figure 12. Kinetic energy gradient (KEG) for the (a) unvegetated and (b) vegetated channels. Vegetation patches shown in green. [Colour figure can be viewed at wileyonlinelibrary.com]

there is evidence from several ADV locations that wake magnitudes are being correctly predicted suggesting that the effect of the vegetation may be represented correctly (e.g. 1 to 2 m, XS1 in Figure 6), and conversely there are also regions where poor model performance appears not to be due to the vegetation model (e.g. 0 to 1 m, XS2 in Figure 6). Instead, it is likely that some modelling errors are due to the coarse grid discretization and simplistic boundary conditions.

The current model presented here treats vegetation patches as static blockages. In nature, vegetation patches may reconfigure to the flow, a process that has been shown to impact upon roughness (Siniscalchi and Nikora, 2013; Verschoren *et al.*, 2016). Including the effects of patch reconfiguration would permit the application of the model across a wider range of flow conditions but would require further field data to accurately quantify patch reconfiguration across a range of velocities. Furthermore, vegetation canopies may respond dynamically to the local flow field, moving in response to turbulence introduced by canopy shear layers (Ghisalberti and Nepf, 2002) and plant flapping processes (Nikora, 2010). Inclusion of these effects would be possible using a dynamic drag mask (Ikeda *et al.*, 2001; Marjoribanks *et al.*, 2014b), which moves at each timestep. Scales of plant motion could be characterized from the lateral shear layer velocity profiles evident within the time-averaged velocity field and using data from the ADV measurements collected in the field. However, such an improvement would require a time-dependent flow calculation that itself incurs higher computational cost through finer grid resolutions and high frequency time-stepping. Assessing the impact of these dynamic flow–vegetation interactions on patch-scale hydraulics is a direction for future research.

Considering these factors, and the ability of the model to reproduce the shape of the velocity profiles and velocity magnitude at the ADV locations, we suggest that the model presented here provides a promising methodology for predicting the patch-scale effect of vegetation on flow within rivers. In particular, the model provides a wealth of spatial data that existing flow–vegetation models are not able to provide, and may have a role in river management, especially in conservation areas such as chalk rivers where there is a fine balance between the demands of flood and ecosystem management (Cranston and Darby, 2004).

Conclusion

This paper has outlined a new patch-scale representation of vegetation within a CFD model that is capable of representing static, submerged aquatic vegetation through a combined drag and MFSA treatment. The model has been shown to produce key flow structures associated with vegetated channels including wake regions and high velocity threads and shows improved accuracy with resolution, achieving <5% error for reach-scale hydraulic measures at 0.05 m resolution.

Further work is required to assess and improve the accuracy of the model across a range of flow and vegetation conditions and to assess the impact of temporal flow and vegetation dynamics on flow predictions. Nevertheless, we show that this model provides new capabilities for assessing the effect of vegetation on rivers, including its impact on hydraulics as well as sediment transport and ecology.

References

Albayrak I, Nikora V, Miler O, O'Hare M. 2014. Flow–plant interactions at leaf, stem and shoot scales: drag, turbulence, and biomechanics. *Aquatic Sciences* **76**: 269–294. DOI:10.1007/s00027-013-0335-2.

Baptist MJ, Babovic V, Rodríguez Uthurburu J, Keijzer M, Uittenbogaard RE, Mynett A, Verwey A. 2007. On inducing equations for vegetation resistance. *Journal of Hydraulic Research* **45**: 435–450. DOI:10.1080/00221686.2007.9521778.

Boussinesq J. 1877. *Essai sur la théorie des eaux courantes*. Mémoires présentes pars divers savants à l'Académie des Sciences: Paris.

Bovee KD. 1978. The incremental method of assessing habitat potential for coolwater species, with management implications. *American Fisheries Society Special Publication* **11**: 340–343.

Bradbrook KF, Lane SN, Richards KS. 2000. Numerical simulation of three-dimensional, time-averaged flow structure at river channel confluences. *Water Resources Research* **36**: 2731–2746. DOI:10.1029/2000wr900011.

Buffin-Bélanger T, Roy AG. 2005. 1 min in the life of a river: selecting the optimal record length for the measurement of turbulence in fluvial boundary layers. *Geomorphology* **68**: 77–94. DOI:10.1016/j.geomorph.2004.09.032.

Carney SK, Bledsoe BP, Gessler D. 2006. Representing the bed roughness of coarse-grained streams in computational fluid dynamics. *Earth Surface Processes and Landforms* **31**: 736–749. DOI:10.1002/esp.1274.

Chen Z, Ortiz A, Zong L, Nepf H. 2012. The wake structure behind a porous obstruction and its implications for deposition near a finite patch of emergent vegetation. *Water Resources Research* **48**: W09517. DOI:10.1029/2012WR012224.

Chow V-T. 1959. *Open Channel Hydraulics.* McGraw-Hill College: New York.

Cokgor S, Kucukali S. 2004. Oxygen transfer in flow around and over stones placed in a laboratory flume. *Ecological Engineering* **23**: 205–212. DOI:10.1016/j.ecoleng.2004.09.004.

Cotton JA, Wharton G, Bass JAB, Heppell CM, Wotton RS. 2006. The effects of seasonal changes to in-stream vegetation cover on patterns of flow and accumulation of sediment. *Geomorphology* **77**: 320–334. DOI:10.1016/j.geomorph.2006.01.010.

Cowan WL. 1956. Estimating hydraulic roughness coefficients. *Agricultural Engineering* **37**: 473–475.

Cranston E, Darby E. 2004. *Ranunculus in Chalk Rivers, Phase 2*, Environment Agency Research and Development Technical Report. Environment Agency Research and Development: London.

Crowder DW, Diplas P. 2000. Evaluating spatially explicit metrics of stream energy gradients using hydrodynamic model simulations. *Canadian Journal of Fisheries and Aquatic Sciences* **57**: 1497–1507. DOI:10.1139/f00-074.

Crowder DW, Diplas P. 2006. Applying spatial hydraulic principles to quantify stream habitat. *River Research and Applications* **22**: 79–89. DOI:10.1002/rra.893.

Dawson FH. 1981. The downstream transport of fine material and the organic-matter balance for a section of a small chalk stream in southern England. *Journal of Ecology* **69**: 367–380. DOI:10.2307/2259673.

de Lima PS, Janzen J, Nepf H. 2015. Flow patterns around two neighboring patches of emergent vegetation and possible implications for deposition and vegetation growth. *Environmental Fluid Mechanics* **15**: 881–898. DOI:10.1007/s10652-015-9395-2.

Ferguson R. 2007. Flow resistance equations for gravel- and boulder-bed streams. *Water Resources Research* **43**: W05427. DOI:10.1029/2006wr005422.

Ferguson RI, Parsons DR, Lane SN, Hardy RJ. 2003. Flow in meander bends with recirculation at the inner bank. *Water Resources Research* **39**: 1322. DOI:10.1029/2003wr001965.

Fischer-Antze T, Stoesser T, Bates P, Olsen NRB. 2001. 3D numerical modelling of open-channel flow with submerged vegetation. *Journal of Hydraulic Research* **39**: 303–310.

Fisher K. 1992. *The Hydraulic Roughness of Vegetated Channels*, Report SR305. Hydraulics Research Ltd: Wallingford.

Folkard AM. 2011. Vegetated flows in their environmental context: a review. *Proceedings of the Institution of Civil Engineers – Engineering and Computational Mechanics* **164**: 3–24. DOI:10.1680/eacm.8.00006.

Ghisalberti M, Nepf HM. 2002. Mixing layers and coherent structures in vegetated aquatic flows. *Journal of Geophysical Research, Oceans* **107**: 11. DOI:10.1029/2001jc000871.

Ghisalberti M, Nepf HM. 2006. The structure of the shear layer in flows over rigid and flexible canopies. *Environmental Fluid Mechanics* **6**: 277–301. DOI:10.1007/s10652-006-0002-4.

Gore JA, Hamilton SW. 1996. Comparison of flow-related habitat evaluations downstream of low-head weirs on small and large fluvial ecosystems. *Regulated Rivers: Research & Management* **12**: 459–469. DOI:10.1002/(SICI)1099-1646(199607)12:4/5<459::AID-RRR413>3.0.CO;2-T.

Green JC. 2005a. Comparison of blockage factors in modelling the resistance of channels containing submerged macrophytes. *River Research and Applications* **21**: 671–686. DOI:10.1002/rra.854.

Green JC. 2005b. Modelling flow resistance in vegetated streams: review and development of new theory. *Hydrological Processes* **19**: 1245–1259.

Green JC. 2006. Effect of macrophyte spatial variability on channel resistance. *Advances in Water Resources* **29**: 426–438. DOI:10.1016/j.advwatres.2005.05.010.

Gurnell A, Tockner K, Edwards P, Petts G. 2005. Effects of deposited wood on biocomplexity of river corridors. *Frontiers in Ecology and the Environment* **3**: 377–382. DOI:10.2307/3868587.

Gurnell AM, van Oosterhout MP, de Vlieger B, Goodson JM. 2006. Reach–scale interactions between aquatic plants and physical habitat: River Frome, Dorset. *River Research and Applications* **22**: 667–680. DOI:10.1002/rra.929.

Hardy RJ, Lane SN, Ferguson RI, Parsons DR. 2003. Assessing the credibility of a series of computational fluid dynamic simulations of open channel flow. *Hydrological Processes* **17**: 1539–1560. DOI:10.1002/hyp.1198.

Hardy RJ, Lane SN, Lawless MR, Best JL, Elliott L, Ingham DB. 2005. Development and testing of a numerical code for treatment of complex river channel topography in three-dimensional CFD models with structured grids. *Journal of Hydraulic Research* **43**: 468–480.

Hodskinson A, Ferguson RI. 1998. Numerical modelling of separated flow in river bends: model testing and experimental investigation of geometric controls on the extent of flow separation at the concave bank. *Hydrological Processes* **12**: 1323–1338. DOI:10.1002/(sici)1099-1085(19980630)12:8<1323::aid-hyp617>3.0.co;2-s.

Ikeda S, Yamada T, Toda Y. 2001. Numerical study on turbulent flow and honami in and above flexible plant canopy. *International Journal of Heat and Fluid Flow* **22**: 252–258.

Jarvela J. 2002. Flow resistance of flexible and stiff vegetation: a flume study with natural plants. *Journal of Hydrology* **269**: 44–54.

Kadlec RH, Knight RL. 1996. *Treatment Wetlands*. Lewis Publishers: Boca Raton, FL.

Kemp JL, Harper DM, Crosa GA. 2000. The habitat-scale ecohydraulics of rivers. *Ecological Engineering* **16**: 17–29. DOI:10.1016/S0925-8574(00)00073-2.

Keylock CJ, Hardy RJ, Parsons DR, Ferguson RI, Lane SN, Richards KS. 2005. The theoretical foundations and potential for large-eddy simulation (LES) in fluvial geomorphic and sedimentological research. *Earth-Science Reviews* **71**: 271–304.

Kim SJ, Stoesser T. 2011. Closure modeling and direct simulation of vegetation drag in flow through emergent vegetation. *Water Resources Research* **47** . DOI:10.1029/2011wr010561.W10511

Kouwen N, Unny TE. 1973. Flexible roughness in open channels. *Journal of Hydraulics Division, ASCE* **101**: 194–196.

Kozarek JL, Hession WC, Dolloff CA, Diplas P. 2010. Hydraulic complexity metrics for evaluating in-stream brook trout habitat. *Journal of Hydraulic Engineering* **136**: 1067–1076. DOI:10.1061/(ASCE)HY.1943-7900.0000197.

Lane SN. 1998. Hydraulic modelling in hydrology and geomorphology: a review of high resolution approaches. *Hydrological Processes* **12**: 1131–1150.

Lane SN, Richards KS, Chandler JH. 1994. Developments in monitoring and modelling small-scale river bed topography. *Earth Surface Processes and Landforms* **19**: 349–368. DOI:10.1002/esp.3290190406.

Lane SN, Hardy RJ, Elliott L, Ingham DB. 2002. High-resolution numerical modelling of three-dimensional flows over complex river bed topography. *Hydrological Processes* **16**: 2261–2272. DOI:10.1002/hyp.5034.

Lane SN, Hardy RJ, Elliott L, Ingham DB. 2004. Numerical modeling of flow processes over gravelly surfaces using structured grids and a numerical porosity treatment. *Water Resources Research* **40**: 18.

Leclerc M. 2005. Ecohydraulics: a new interdisciplinary frontier for CFD. In *Computational Fluid Dynamics*. John Wiley & Sons: Chichester; 429–460.

Lien FS, Leschziner MA. 1994. Assessment of turbulence-transport models including non-linear rng eddy-viscosity formulation and second-moment closure for flow over a backward-facing step. *Computers & Fluids* **23**: 983–1004.

Liu C, Shen Y-m. 2008. Flow structure and sediment transport with impacts of aquatic vegetation. *Journal of Hydrodynamics, Series B* **20**: 461–468.

Liu D, Diplas P, Fairbanks JD, Hodges CC. 2008. An experimental study of flow through rigid vegetation. *Journal of Geophysical Research* **113** . DOI:10.1029/2008jf001042.F04015

López F, García M. 1998. open-channel flow through simulated vegetation: suspended sediment transport modeling. *Water Resources Research* **34**: 2341–2352. DOI:10.1029/98wr01922.

López F, García MH. 2001. Mean flow and turbulence structure of open-channel flow through non-emergent vegetation. *Journal of Hydraulic Engineering ASCE* **127**: 392–402.

Marjoribanks TI, Hardy RJ, Lane SN. 2014a. The hydraulic description of vegetated river channels: the weaknesses of existing formulations and emerging alternatives. *Wiley Interdisciplinary Reviews: Water* **1**: 549–560. DOI:10.1002/wat2.1044.

Marjoribanks TI, Hardy RJ, Lane SN, Parsons DR. 2014b. High-resolution numerical modelling of flow–vegetation interactions. *Journal of Hydraulic Research* **52**: 775–793. DOI:10.1080/00221686.2014.948502.

Meire DWSA, Kondziolka JM, Nepf HM. 2014. Interaction between neighboring vegetation patches: Impact on flow and deposition. *Water Resources Research* **50**: 3809–3825. DOI:10.1002/2013WR015070.

Naden P, Rameshwaran P, Mountford O, Robertson C. 2006. The influence of macrophyte growth, typical of eutrophic conditions, on river flow velocities and turbulence production. *Hydrological Processes* **20**: 3915–3938. DOI:10.1002/hyp.6165.

Nepf HM. 1999. Drag, turbulence, and diffusion in flow through emergent vegetation. *Water Resources Research* **35**: 479–489.

Nepf H, Ghisalberti M, White B, Murphy E. 2007. Retention time and dispersion associated with submerged aquatic canopies. *Water Resources Research* **43**: 10. DOI:10.1029/2006wr005362.

Nepf H, Rominger J, Zong L. 2013. Coherent flow structures in vegetated channels. In *Coherent Flow Structures at Earth's Surface*. John Wiley & Sons: Chichester; 135–147.

Nicholas AP. 2001. Computational fluid dynamics modelling of boundary roughness in gravel-bed rivers: an investigation of the effects of random variability in bed elevation. *Earth Surface Processes and Landforms* **26**: 345–362. DOI:10.1002/esp.178.

Nikora V. 2010. Hydrodynamics of aquatic ecosystems: An interface between ecology, biomechanics and environmental fluid mechanics. *River Research and Applications* **26**: 367–384. DOI:10.1002/rra.1291.

O'Hare MT, McGahey C, Bissett N, Cailes C, Henville P, Scarlett P. 2010. Variability in roughness measurements for vegetated rivers near base flow, in England and Scotland. *Journal of Hydrology* **385**: 361–370.

Okamoto TA, Nezu I. 2009. Turbulence structure and 'Monami' phenomena in flexible vegetated open-channel flows. *Journal of Hydraulic Research* **47**: 798–810. DOI:10.3826/jhr.2009.3536.

Olsen NRB, Stokseth S. 1995. 3-dimensional numerical modelling of water-flow in a river with large bed roughness. *Journal of Hydraulic Research* **33**: 571–581.

Sand-Jensen K. 1998. Influence of submerged macrophytes on sediment composition and near-bed flow in lowland streams. *Freshwater Biology* **39**: 663–679. DOI:10.1046/j.1365-2427.1998.00316.x.

Sand-Jensen KAJ, Jeppesen E, Nielsen K, Van Der Bijl L, Hjermind L, Nielsen LW, Ivlrsln TM. 1989. Growth of macrophytes and ecosystem consequences in a lowland Danish stream. *Freshwater Biology* **22**: 15–32. DOI:10.1111/j.1365-2427.1989.tb01080.x.

Shucksmith JD, Boxall JB, Guymer I. 2011. Bulk flow resistance in vegetated channels: analysis of momentum balance approaches based

on data obtained in aging live vegetation. *Journal of Hydraulic Engineering* **137**: 1624–1635.

Siniscalchi F, Nikora V. 2013. Dynamic reconfiguration of aquatic plants and its interrelations with upstream turbulence and drag forces. *Journal of Hydraulic Research* **51**: 46–55. DOI:10.1080/00221686.2012.743486.

Sotiropoulos F. 2005. Introduction to statistical turbulence modelling for hydraulic engineering flows. In *Computational Fluid Dynamics: Applications in Environmental Hydraulics*, Bates P, Lane SN, Ferguson RI (eds). John Wiley & Sons: Chichester.

Spalding DB. 1980. *Mathematical Modelling of Fluid Mechanics, Heat Transfer and Mass Transfer Processes*. Mechanical Engineering Department, Imperial College of Science, Technology and Medicine: London.

Stoesser T, Wilson CAME, Bates PD, Dittrich A. 2003. Application of a 3D numerical model to a river with vegetated floodplains. *Journal of Hydroinformatics* **5**: 99–112.

Sukhodolov AN, Sukhodolova TA. 2010. Case study: effect of submerged aquatic plants on turbulence structure in a lowland river. *Journal of Hydraulic Engineering* **136**: 434–446.

Verschoren V, Meire D, Schoelynck J, Buis K, Bal K, Troch P, Meire P, Temmerman S. 2016. Resistance and reconfiguration of natural flexible submerged vegetation in hydrodynamic river modelling. *Environmental Fluid Mechanics* **16**: 245. DOI:10.1007/s10652-015-9432-1.

Westlake. 1975. Macrophytes. In *River Ecology*, Whitton BA (ed). University of California Press: Berkeley, CA.

Wilson NR, Shaw RH. 1977. A higher order closure model for canopy flow. *Journal of Applied Meteorology* **16**: 1197–1205. DOI:10.1175/1520-0450(1977)016<1197:ahocmf>2.0.co;2.

Wilson CAME, Stoesser T, Bates P. 2005. Modelling of open channel flow through vegetation. In *Computational Fluid Dynamics: Applications in Environmental Hydraulics*, Bates P, Lane SN, Ferguson RI (eds). John Wiley & Sons: Chichester.

Yakhot V, Orszag SA. 1986. Renormalization group analysis of turbulence. I. Basic theory. *Journal of Scientific Computing* **1**: 3–51. DOI:10.1007/bf01061452.